ARL

Bioeffects on an In Vitro Model by Small-Scale Explosives and Shock Wave Overpressure Impacts

by Nicole E Zander, Thuvan Piehler, Rohan Banton, and Richard Benjamin

NOTICES

Disclaimers

The findings in this report are not to be construed as an official Department of the Army position unless so designated by other authorized documents.

Citation of manufacturer's or trade names does not constitute an official endorsement or approval of the use thereof.

Destroy this report when it is no longer needed. Do not return it to the originator.

US Army Research Laboratory

Bioeffects on an In Vitro Model by Small-Scale Explosives and Shock Wave Overpressure Impacts

by Nicole E Zander, Thuvan Piehler, Rohan Banton, and Richard Benjamin
Weapons and Materials Research Directorate, ARL

REPORT DOCUMENTATION PAGE		*Form Approved* *OMB No. 0704-0188*
Public reporting burden for this collection of information is estimated to average 1 hour per response, including the time for reviewing instructions, searching existing data sources, gathering and maintaining the data needed, and completing and reviewing the collection information. Send comments regarding this burden estimate or any other aspect of this collection of information, including suggestions for reducing the burden, to Department of Defense, Washington Headquarters Services, Directorate for Information Operations and Reports (0704-0188), 1215 Jefferson Davis Highway, Suite 1204, Arlington, VA 22202-4302. Respondents should be aware that notwithstanding any other provision of law, no person shall be subject to any penalty for failing to comply with a collection of information if it does not display a currently valid OMB control number. **PLEASE DO NOT RETURN YOUR FORM TO THE ABOVE ADDRESS.**		

1. REPORT DATE *(DD-MM-YYYY)*	2. REPORT TYPE	3. DATES COVERED (From - To)
November 2017	Technical Report	1 June 2015–1 August 2016

4. TITLE AND SUBTITLE	5a. CONTRACT NUMBER
Bioeffects on an In Vitro Model by Small-Scale Explosives and Shock Wave Overpressure Impacts	
	5b. GRANT NUMBER
	5c. PROGRAM ELEMENT NUMBER
6. AUTHOR(S)	5d. PROJECT NUMBER
Nicole E Zander, Thuvan Piehler, Rohan Banton, and Richard Benjamin	
	5e. TASK NUMBER
	5f. WORK UNIT NUMBER

7. PERFORMING ORGANIZATION NAME(S) AND ADDRESS(ES)	8. PERFORMING ORGANIZATION REPORT NUMBER
US Army Research Laboratory ATTN: RDRL-WMM-G Aberdeen Proving Ground, MD 21005-5066	ARL-TR-8210

9. SPONSORING/MONITORING AGENCY NAME(S) AND ADDRESS(ES)	10. SPONSOR/MONITOR'S ACRONYM(S)
	11. SPONSOR/MONITOR'S REPORT NUMBER(S)

12. DISTRIBUTION/AVAILABILITY STATEMENT

Approved for public release; distribution is unlimited.

13. SUPPLEMENTARY NOTES

14. ABSTRACT

Despite many years of research, the effect of blast waves on brain tissues and cells remains incompletely understood. In vitro and in vivo laboratory models have proven useful in delineating some of the biological effects and mechanisms related to damage. We reported here the bioeffects of peak pressure impacts from shock tube and explosive charges on dissociated brain cells (NG108-15 cells), a fusion of mouse neuroblastoma and rat glioma cells. The pressure waves were generated from a shock tube and small-scale open-air explosive charges. The cell plates were submerged under water for the explosive blast condition, while the cell plates remained in air for the shock tube condition. NG108-15 cells were exposed to single or triple shock/blast waves. Compared to sham-treated conditions, cells that were either submerged in a water tank and exposed to a small-scale explosive or placed in the shock tube were found to have altered membrane permeability, intracellular calcium and sodium ion levels, and elevated oxidative stress. In comparing the 2 methods of shock/blast wave exposure, the most significant difference observed was in membrane permeability. NG108-15 cells subjected to blast by a shock tube had 2 to nearly 4 times higher uptake of calcein dye for single and repeated blast compared to those exposed to explosive blast at the same peak pressure. In addition, oxidative stress, and intracellular sodium and calcium ion levels were significantly higher for cells exposed to shock tube blasts compared to live explosive blast. These differences are perhaps related to the larger impulse generated by the shock tube, compared to the blast wave that traversed the cells submerged in the water tank.

15. SUBJECT TERMS

primary blast, mild traumatic brain injury, in vitro model, repetitive blast, shock tube, explosives

16. SECURITY CLASSIFICATION OF:			17. LIMITATION OF ABSTRACT	18. NUMBER OF PAGES	19a. NAME OF RESPONSIBLE PERSON
					Nicole E Zander
a. REPORT	b. ABSTRACT	c. THIS PAGE	UU	34	19b. TELEPHONE NUMBER (Include area code)
Unclassified	Unclassified	Unclassified			410-306-1965

Contents

List of Figures

List of Tables

Acknowledgments

1.   Introduction

Traumatic brain injury (TBI) remains one of the signature injuries of the current conflicts and affects upwards of 20% of deployed military personnel.[1] Many TBIs are associated with blast from improvised explosive devices.[2–4] Explosions are physical, chemical, or nuclear reactions involving a rapid release of large amounts of energy, generating a substantial rise in pressure in the immediate vicinity. The overpressure phase typically lasts for a few microseconds to seconds and is followed by a negative pressure phase or vacuum in which surrounding air is pulled toward the explosion source.[5] The exploding ordinance can injure the exposed party in 4 ways. Primary injuries or pure blast injuries result from the transmission of the blast wave through the body, mainly affecting organs and cavities such as the lung and ears. Secondary, tertiary, and quaternary injuries involve fragment penetration, head or body acceleration, and burns or chemical gas exposure, respectively.[6]

During an explosive blast, there is a partition of energy in the propagating waves between static or overpressure that causes compression of a target, and dynamic pressure that causes displacement or movement of the target. The negative phase of a blast wave can cause suction and the flow of the air to reverse, with material being swept toward the blast source. Upon exposure to a blast wave, the target is enveloped in the blast wave, which creates a wrap-around effect. Reproduction of each part of the open air explosive phenomena is critical for blast injury models.[7]

A number of test methods are commonly used to simulate shock/blast waves from high explosives, including open air/free-field explosives, shock tubes, and blast tubes.[6] To produce relevant blast-related injuries, proper replication of blast wave forms, including peak overpressure, pressure time history, exposure duration, and post-blast wind, is important. Shock tubes are currently widely used as blast-wave simulators. The key advantages of shock tubes are reduced cost, improved reproducibility, and ease of use in a controlled laboratory environment. The compressed air-driven shock tube is a horizontally mounted square, or circular steel tube, with a closed end. A gas at low pressure (driven gas) is separated from a gas at high pressure (driving gas) by a diaphragm such as a Mylar membrane. The diaphragm is ruptured by increasing the pressure difference between the 2 sections, and the overpressure propagates along the length of the tube. Some shock tubes are driven by the detonation of an explosive charge in the closed end of the tube.[8] Pressure can be adjusted by the number of membranes inserted between the 2 pressure regions in the shock tube or the size and type of detonation, respectively.[9] Both types of shock tubes have been shown to cause injury in in vitro and in vivo experiments.[9–12]

The main disadvantage of shock tubes is that they can potentially generate complicated reflected shock waves. Complications in interpretation can result from shock tube designs that cause this series of complex shock waves in the confined shock tube, including reflected shock waves, Mach stem, an unsteady turbulent jet, and rarefaction waves.[8] It should be noted that explosives can also generate complex blast pressure waves when detonated in closed environments. In addition, these complex shock waves from certain shock tubes can cause more severe injuries than those observed in blast victims due to the sudden compression or rarefaction events and transfer of kinetic energy to the target.[8,13] The position of the animal or sample and the size of the animal or sample relative to the shock tube or percentage of cross-sectional area of the shock tube blocked are also critical to consider, as these parameters can improve or decrease the value of the experiments.[7,14] In addition, the pressure profiles change along the length of the shock tube.[15] For the research described here, we have used the recently developed, optimally designed Advanced Blast Simulator (ABS). It is considered the state-of-the-art shock tube designed to replicate key features of the blast wave, including the negative pressure phase.[16]

On another hand, explosive blast experiments must also be carefully designed with proper positioning of explosives and sample. For indoor experiments, the distance from the walls and ceiling must be considered, as they can generate reflected waves not representative of open air explosive blasts. The experiments in this work were done indoors in an aquarium tank filled with water. While the distance from the walls and ceilings was large enough for reflections off the surfaces to be considered negligible, reflections were generated from the walls of the aquarium tank. Hence, the use of appropriate and accurate models to simulate blast injury or at least an understanding of a model's shortcomings is critical for improved understanding of the mechanisms of injury, which are still poorly understood, and proper diagnosis and treatment.[17]

Many TBIs—in particular, mild TBIs (mTBI)—seldom have neuroanatomical abnormalities detectable by conventional imaging methods such as magnetic resonance imaging.[18] Thus, self-reporting of symptoms is the main mechanism of diagnosis of mTBI. Many in vitro models report changes in membrane permeability, either transient or permanent, to be a significant contributor to blast-induced cellular injury.[19–21] The openings in the membrane allow for increased ionic transport, particularly sodium, which can in turn cause a rise in intracellular calcium.[22] A host of pathways leading to compromised cellular structure and function can be activated. These include ionic imbalance such as osmotic swelling and cytoskeletal damage, axonal beading, and focal adhesion complex disruptions.[23] Increased oxidative stress is another potential outcome from blast

exposure frequently investigated using in vitro and in vivo models of blast-induced mTBI. Oxidative stress can lead to mitochondrial dysfunction as well as inflammation pathways that ultimately lead to neuronal degeneration.[24]

In this work, we studied single and repeated blast effects of shock tube with that of small-scale open-air explosives on NG108-15 cells. The cell samples were plated in plastic plates under growth media and submerged in a water tank (explosive blast) and in air (shock tube). While direct comparisons cannot be made, conditions were optimized to match peak overpressure and minimize movement of the specimens in both experiments. Since cell death was found to be minimal at the pressure evaluated, changes in membrane permeability, intracellular sodium, intracellular calcium, and reactive oxygen species were probed.

2.   Materials and Methods

2.1 Culture of NG108-15 Cells

NG108-15 cells, a fusion of mouse N188TG2 neuroblastoma cells with rat C6-BU-1 glioma cells, were obtained from ATCC (ATCC HB-12317) and used at passage numbers of 20–30. Cells were grown in Dulbecco's Modified Eagle's Medium (ThermoFisher, 12100061) supplemented with 0.1 mM hypoxanthine, 400 nM aminopterin, 0.016 mM thymidine (ThermoFisher, 21060017), 10% fetal bovine serum (ThermoFisher), 1.5 g/L sodium bicarbonate (Sigma Aldrich), and Penicillin/streptomycin (1% v/v, Corning). Cells were maintained at 37 °C in a humidified incubator with 5% CO_2 in air. Cells were plated in 24-well tissue culture polystyrene dishes. After 24 h of incubation, half of the media was removed and replaced with fresh media. Media changes were repeated every 2 days until the day of experiment (day 5 in culture). It is important to note that in order not to contaminate or interrupt the dissociated neurons in the 24-well plate, no experimental pressure probes were placed inside the wells.

2.2 Open-Air Explosive Blast-Induced Injury of Cells (in Water)

Just prior to the blast experiment, sterile HEPES buffer (10 mM; Sigma-Aldrich) was added, and the well plates were sealed with sterile SealPlate covers from Excel Scientific. The samples were transported to the blast site and held in an incubator at 37 °C until the experiments. The details of the blast experiment have been previously described.[25] In brief, cell culture well plates were mounted, secured, and immersed horizontally in a 10-gal poly(methyl methacrylate) (PMMA) aquarium containing water heated to 37 °C, as displayed in Fig. 1A and Fig. 2A-B. The charge standoff distance was adjusted to generate ca. 140 kPa side-on pressures measured

50 mm above the center of the culture plates by 3 pressure gauges separated 1 inch apart (350 mm, measured from explosive charge to pressure sensors above the center of the well plate). Previous experiments have shown that peak pressure can be reproduced with standard deviations between 6% and 28% (of the pressure value).[25] The average intensity of the blast wave across the sample plate was the same for the single and repeated blasts (125 ± 24 kPa).[25] The single blast was conducted first followed by the repeated blast. Multiple blasts were separated by 5- to 7-min intervals during which the samples were not removed from the tank. This exposure time was chosen to minimize the time cells were out of the incubator and cost of the experiments, and does not necessarily reflect actual battlefield exposure conditions. Spherical 1.7 g/cm^3 cyclotrimethylene trinitramine Class 5 (RDX Class V) charges with hemispherical morphology were used to generate the blast.
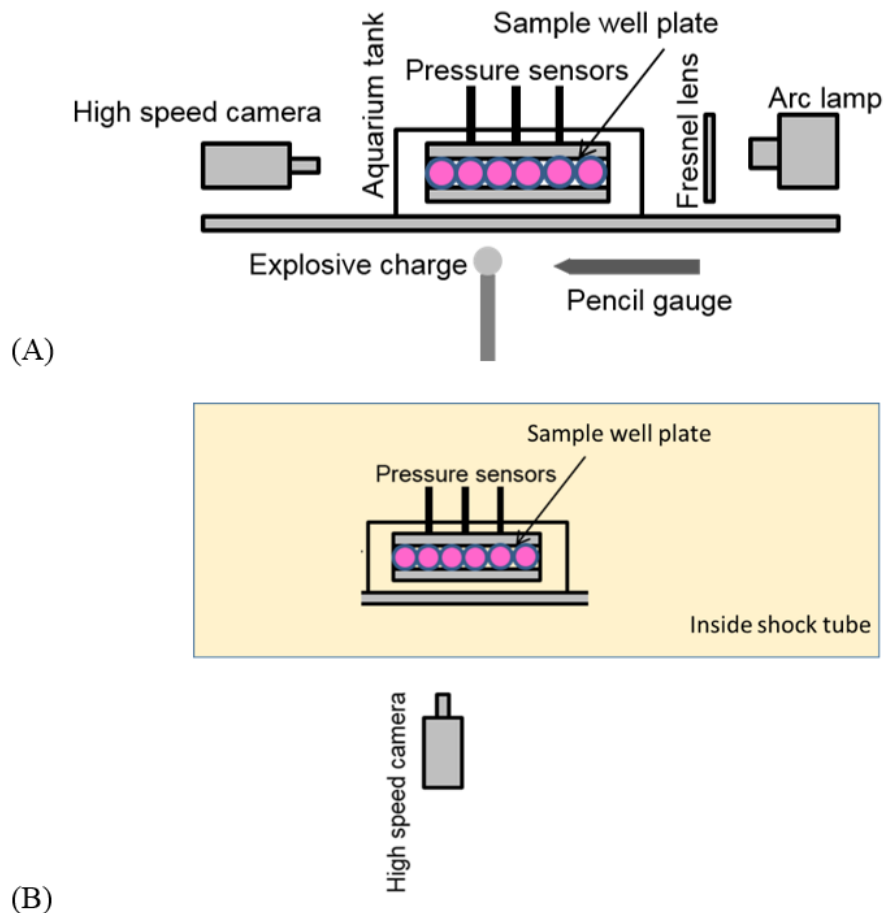
Fig. 1   **Schematic of experiment models: (A) Explosive blast–induced cellular injury model. Reproduced with permission.[26] (B) Shock tubed–induced cellular injury model.**
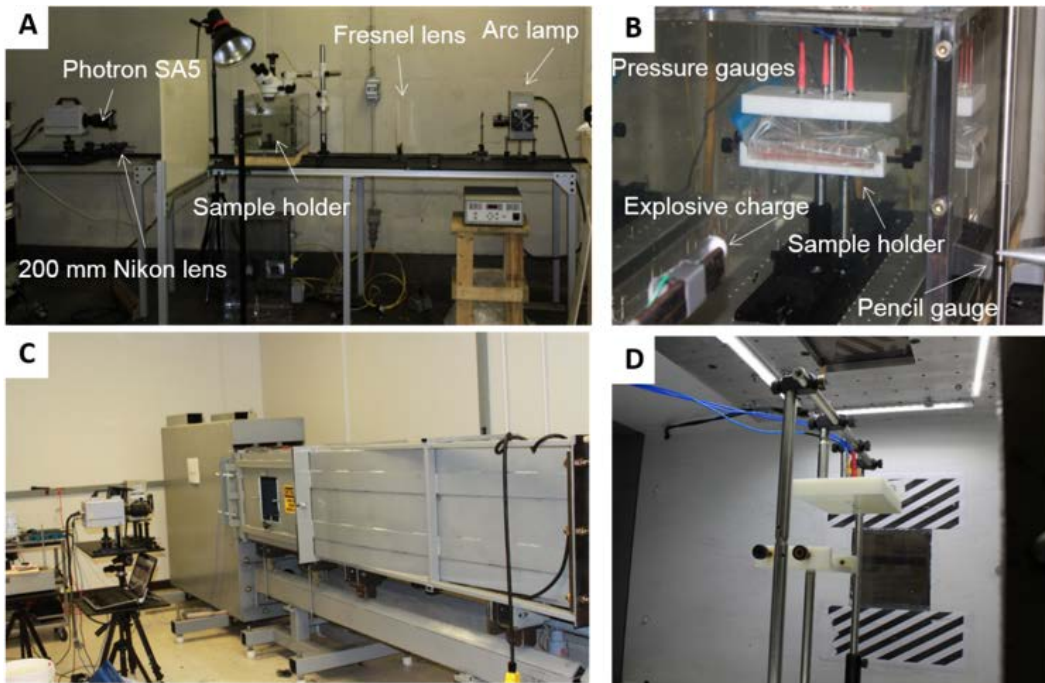
Fig. 2   Primary blast–induced injury of cells: (A) Open-air explosive setup showing high-speed camera, aquarium tank, focusing lens, and light source; (B) Sample plate submerged in aquarium tank showing locations of pressure sensors 2 inches above lid, and explosive charge and pencil gauges outside of tank; (C) Advanced Blast Simulator air-driven shock tube; (D) Sample holder location in a shock tube showing the location of pressure sensors.

2.3 Shock Tube Induced Injury of Cells (in Air)

The ABS (ORA, Inc., Fredericksburg, VA) consists of 4 sections: high-pressure driver, transition section, test section, and end wave eliminator/muffler, and was used to expose the cells to simulated blast wave (Fig. 1B and 2C-D). Membranes consisting of acetate sheets (0.254 mm thick, Grafix Plastics, Cleveland, OH) and plastic mesh (Pet screen, Cat. No. 70589, New York Wire, Hanover, PA) were placed between the high-pressure driver and transition sections, and compressed air was used to pressurize the high-pressure driver. The blast wave was generated when the membrane burst, and as a result of the gradual widening of the transition section, the shock wave takes a planar form. The blast waveform at the center of the test section resembled a theoretical Friedlander curve. The samples were mounted inside the shock tube in air using the same holder used underwater for the explosive experiments. Eight shots were performed for this study with 3 sheets of acetate film. The average intensity of the side-on blast wave across the sample plate was the same for the single and repeated blasts (152 ± 11 kPa). A single blast was conducted first followed by the repeated blast. Multiple blasts were separated by 5- to 7-min intervals during which the samples were not removed from the shock tube.

2.4 Computational Modeling

The blast simulations were performed in an Eulerian domain with the computational domain size of 90×105 cm. The computational domains entailed a RDX explosive charge of radius 4.9 mm placed at varying standoff distances from the embedded 24-well plate assembly in the aquarium, which is surrounded by air. Here, the 24-well plate modeled had dimensions of 12.6 cm $\times 8.5$ cm with inscribed circles of radii 0.8 cm to represent each of the 24 wells. The distance between the centers of each well was maintained at 1.95 cm with web thickness between wells of 0.15 cm and well wall thickness of 0.1 cm. In all the simulations conducted, the 24-well plate assembly was centrally placed in the aquarium at a distance of 200 mm from the front wall of the aquarium. The modeled aquarium dimensions used were 53.2 cm $\times 64.8$ cm with wall thickness of 20 mm.

The nonlinear interaction between the blast waves propagating from the RDX explosive that entered the 24-well plate assembly involved solving the governing partial differential equations for conservation of mass, momentum, and energy, in addition to the material constitutive equations, and the initial and boundary conditions. An Eulerian shock physics wave code, CTH[27], was used to carry out the blast simulations performed in this work. CTH used a mesh that was fixed in space where materials flew through the mesh in response to initial and boundary conditions. A second-order accurate Eulerian solution algorithm was used to solve the mass, momentum, and energy conservation equations. These governing equations were solved in a 2-step process involving first a Lagrangian step followed by a second remap step. In the Lagrangian step, a Lagrangian representation of the governing equations was solved explicitly across each time step. The initial mesh was distorted to allow for material motion while not permitting mass flux across the cell boundaries. Subsequently, a remap step was performed where the distorted cells from the prior step are remapped back to the initial fixed mesh.

The CTH code also incorporated a wide variety of material models to account for material response behavior due to large deformation resulting from shock and blast loading. These models involved an equation of state (EOS), a strength model, and a failure model for each material. These models arose from the total stress tensor where it can be decomposed into its hydrostatic stress and deviatoric stress components. The hydrostatic stress component produced changes in volume/density within the material while the deviatoric stress component was responsible for changes in the material shape. An EOS was therefore used to capture changes in the material hydrostatic stress (pressure) through relations with pressure, mass density, and internal energy density/temperature changes. The strength model was used to relate the deviatoric stress component through relations

with material characteristic behavior involving material deformation (i.e., strain, strain rate, and material temperature). A failure model was also used to capture the material failure due to compressive and tensile stresses.

The simulations conducted in this work incorporated EOS and constitutive models from the CTH database library representing the aquarium walls, the enclosed water medium, the embedded 24-well sample plates containing water-filled wells, and the surrounding air medium. The aquarium walls and the 24-well plate assembly were represented as PMMA, where a Mie–Grüneisen EOS was used for the hydrodynamic response and an elastic perfectly plastic strength model for the constitutive behavior. A failure model from the CTH library based on stress fracture was also applied to the PMMA material in the aquarium walls and the 24-well plate assembly. A tabular sesame EOS was used for the surrounding air and the water medium in the aquarium, and in the 24-well plate. The Jones–Wilkens–Lee EOS was used to represent the RDX explosive.[28]

The blast simulations were started using a programmed burn technique to propagate an ideal detonation wave front following point initiation at the center of the 1.7-g charge of the RDX explosive. An adaptive mesh refinement (AMR) technique was used to refine the expanding propagating shock front as it moved through the spatial domain in air, through the aquarium, and in the cell sample assembly. The strength of the pressure waves from the RDX blast through the PMMA, and the subsequent water medium, as well as in each well sample, were investigated using strategically placed tracer particles.

Calculations that were otherwise inaccessible with experimental diagnostics were carried out to determine pressure loading in each well within the 24-well plate assembly. A typical blast simulation was performed for 24 h using 16 processors for time integrated out to 2 ms with 2.8×10^5 cell calculation. All blast simulations were conducted on the US Army Research Laboratory's Excalibur High Performance Computer, a part of the Department of Defense Supercomputing Resource Center.

2.5 Confocal Laser Scanning Microscopy

Samples were imaged using confocal laser scanning microscopy on a Zeiss LSM 700 equipped with Plan-Apochromat lenses. A minimum of $n = 5$ random areas for 3 replicate sample wells for each experiment were imaged (6 images total). The reported n in the figures refers to the total number of cells analyzed for each condition, randomly chosen from the 15 images collected. In general, 6 representative images for each condition were chosen for data processing. All data were collected 24 h after blast exposure. To assess membrane permeability changes,

the cells were washed with Hanks' balanced salt solution (HBSS; Hyclone) and incubated in 0.3 mM calcein (Life Technologies) in HBSS for 10 min at 37 °C, followed by thorough rinsing before analysis. For reactive oxygen species (ROS) evaluation, cells were rinsed with phosphate-buffered saline (PBS) and incubated in 7 µM 6-carboxy-2',7'-dichlorodihydrofluorescein diacetate (Carboxy-H2DCFDA; Life Technologies) for 30 min, followed by rinsing and 30-min recovery, all at 37 °C. For calcium imaging, 50 µg of Fluo-4 was dissolved in 8 mL PBS with 75 µL of pluronic acid/DMSO (0.05 g/mL) (Life Technologies). Cells were rinsed with PBS and incubated in the Fluo-4 solution for 30 min, followed by rinsing and 30-min recovery at 37 °C. For sodium imaging, cells were rinsed with PBS and incubated in 10 µM CoroNa Green (Life Technologies) for 30 min at 37 °C, followed by thorough rinsing before analysis. For the ROS, calcein, calcium, and sodium images, imaging gains and offsets were fixed for each dye to allow semi-quantitative comparison between samples. Fluorescence intensities were measured by selecting individual cells using the region of interest feature and calculating the mean intensity using the histogram feature.

2.6 Statistics

All data are expressed as mean ± standard deviation unless noted. One-way analysis of variance (ANOVA) with a Tukey Means Comparison was conducted with a significance level of $p < 0.05$. Experiments were conducted 2 times for both the explosive blast and shock tube conditions. All experiments were performed with a minimum of 3 replicate wells from the 2 separate experiments. Because the shams for the shock tube and open-air explosive experiments were significantly different for all assays except the oxidative stress assay, significant differences between experiments were determined by normalizing to the respective sham. In brief, fluorescence intensities of the single and triple shots for each assay were divided by their respective average sham fluorescence intensity.

2.7 Numerical Investigation of Blast-Wave Interaction on 24 Well-Plate Assembly in an Aquarium

Computational modeling and simulations were coupled with in vitro experiments to determine the pressure loading experienced in each well of the 24-well plate assembly embedded in an aquarium. Figure 3 shows an example of the blast-induced injury cell experiment (Fig. 3A) and the corresponding computational geometry setup with the RDX explosive standoff from the sample (Fig. 3B). Two-dimensional (2-D) simulations were carried out using a cross-sectional or a "bird-eye" view of the blast wave interactions in the aquarium.
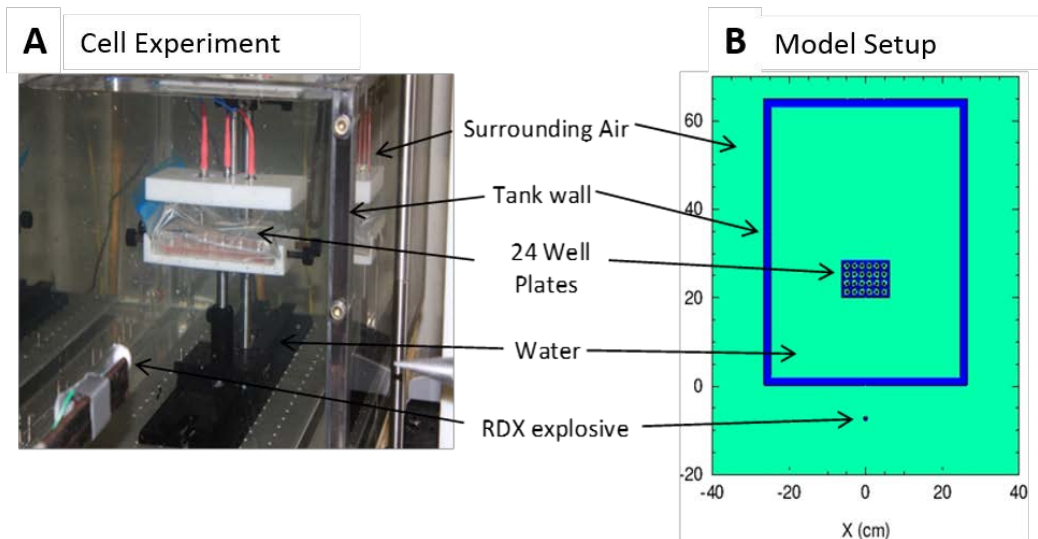
Fig. 3   A) Dissociated neurons in 24-well plate embedded in water-filled aquarium and B) 2-D numerical setup of experiment showing top-down view of 24-well plate immersed in water-medium contained by aquarium walls and surrounded by air with RDX explosive at specified standoff distance.

3.   Results and Discussion

3.1 Numerical Model Results of Blast-Wave Interaction on 24 Well-Plate Assembly in an Aquarium

To gain confidence in the model calculations, blast simulations were compared to the experiments in terms of the pressure history data where no sample wells are included in the aquarium. As an example, simulated results were compared with experimental measurements at a specified distance of 350 mm from the RDX charge. Specifically, the RDX charge was placed 150 mm in front of the aquarium wall with pressure probes placed 200 mm behind the front wall in the water-filled aquarium for a total distance of 350 mm. Figure 4 shows the calculated (red) and experimental (black) pressure histories in water at the standoff distance of 350 mm. The results in Fig. 4 show that both the calculated and recorded pressures are in good agreement with compressive peak pressures of 142.96 kPa and 135.08 kPa, respectively. However the experimental results showed strong early oscillations or ringing of the pressure waves with volumetric tension (negative pressures) reaching magnitudes of 80.25 kPa at 0.267 ms and 89.18 kPa at 0.366 ms. The calculated results also exhibited volumetric tension of magnitude 50 kPa, albeit at later times between 0.427 to 0.479 ms beyond 0.5 ms. Both the recorded and calculated results exhibit reasonable agreement in the oscillations or ringing of the pressure waves.
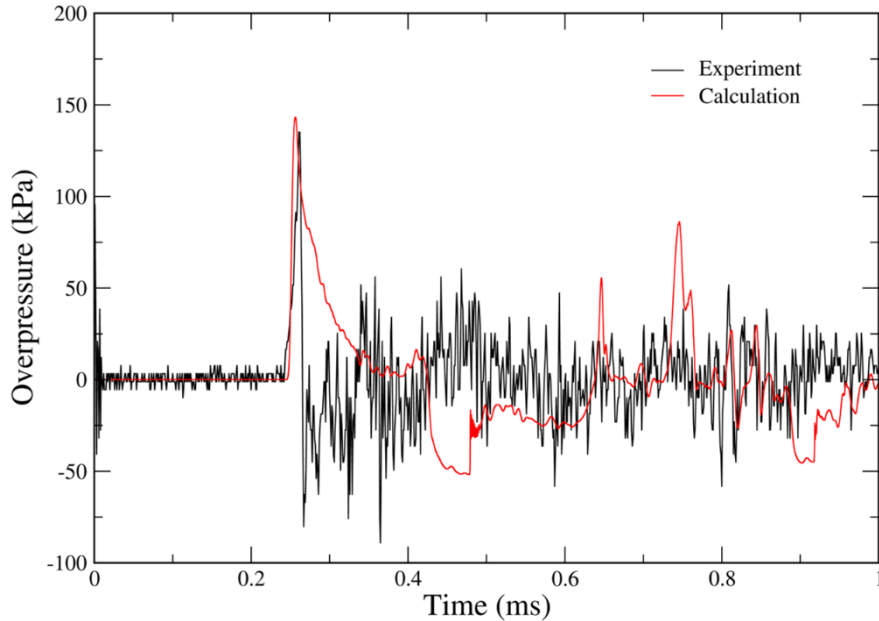
Fig. 4   Model calculations validated with blast experiments showing RDX explosive pressure histories in water-filled aquarium at 350-mm total standoff.

Having validated the numerical model, we used the Eulerain shock physics code CTH to determine pressure–time histories in the 24-well plate that not were not readily accessible with experimental diagnostics. For example, tracer particles were strategically placed in sample wells to determine pressure–time histories resulting from RDX spherical charge–generated blast waves. Because of the symmetry of the shock wave, only 3 tracer particles were used for each row of 6 wells. Results from the computational calculation inside the 24 sample wells are shown in Figs. 5–7. In CTH, the AMR capabilities were used to refine the expanding propagating shock front as it moved through the spatial domain. Figure 5 shows the AMR problem geometry setup with RDX explosive charge standoff at 350 mm from the sample and location of tracer particles. As the explosive charge detonated in air, the AMR refinement techniques were used to resolve the shock front as it moved from air in the aquarium material (PMMA) into the fluid (water) medium. The sequence of pressures of the propagating detonation up to the point of impact is displayed in Fig. 6. Figure 7 shows the pressure histories for the first row of the well plate for the 3 tracer particles. The onset of the blast wave occurred at about 0.247 ms for all tracers, and the input pressures were almost identical (152 kPa for tracers 1, 2, and 3). At a later time, 0.604 ms, the cells experienced strong volumetric tension of about –57.35 kPa followed by multiple reflection compressive loading. Tracer 1 in particular experienced the strongest reflection waves on the order of 145 and 198 kPa for times 0.642 and 0.749 ms, respectively. Similar reflected waves were also exhibited in tracers 2 and 3, albeit at lower loading of about 105 kPa. The pressure

readings from tracers 1, 2, and 3 also exhibited the same trends as our previous work.[25] Figure 7B highlights the drop in pressure histories as the waves propagate across the 24-well plate. The tracer particles were selected along column b for rows 1–4. The input pressures in the wells dropped from 152 kPa in row 1 to 118 kPa in row 4. Secondary reflected compressive waves were also evident but reduced in magnitude across the 24-well plate. A further drop in pressure was more evident in Fig. 7C between tracer 1 in the first row and tracer 24 in the fourth row. Here, a 45-kPa drop in pressure occurred as a wave propagates from the front row to the back of the 24-well plate. In all the cases studied, the input pressure wave was followed by a tensile wave and subsequent reflected waves. The well plate contained areas of plastic, fluid (media), and air gaps that increased the complexity of the model but served as a projected guess of peak pressure in regions that were unable to be measured directly.
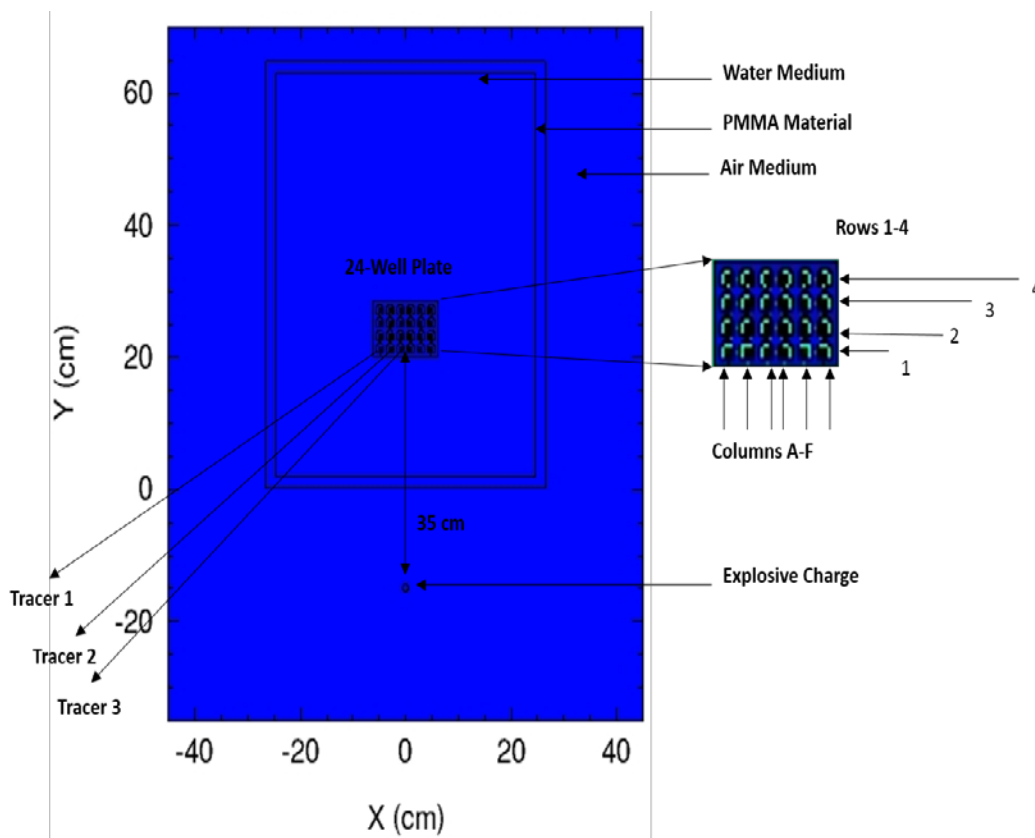
Fig. 5   Computational model setup used to simulate detonation propagation from explosive charge in air to 24-well plate immersed in water medium at a distance of 350 mm from the charge. Tracer particles are denoted as black dots inside the well plates.
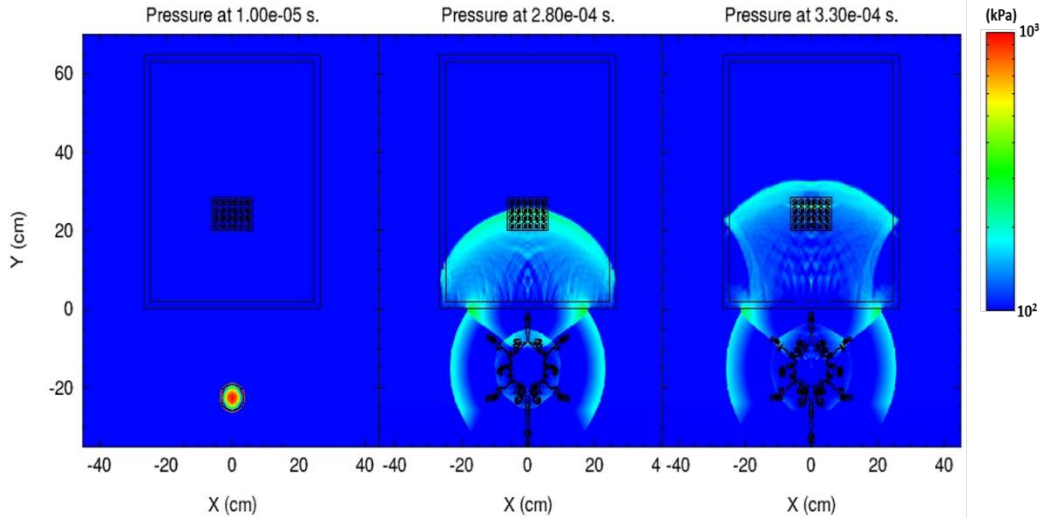
Fig. 6 **Sequence of pressure contours showing detonation propagation from explosive charge in air through PMMA material (tank wall) into water medium containing 24-well plate. Charge standoff distance at 350 mm from the front of the aquarium (tank wall).**
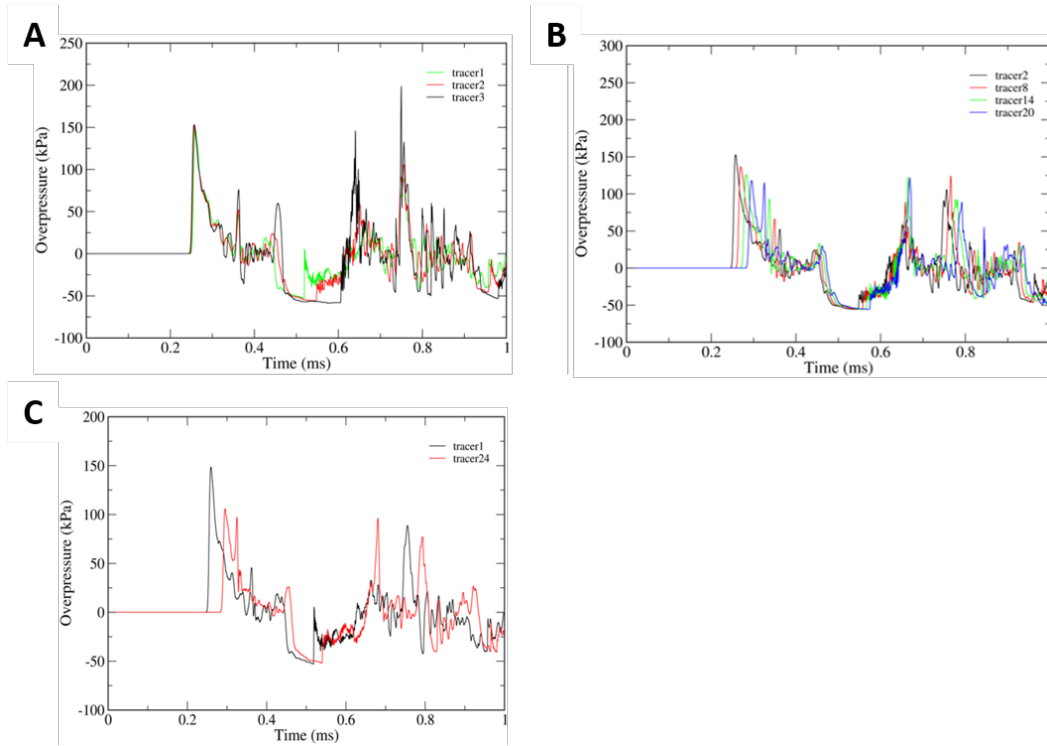
Fig. 7 **(A) Pressure histories in the first row of 24-well plate identified by tracers 1, 2, and 3 in Fig. 5. Pressure histories showed an input pressure of 152 kPa followed by strong multiple compressive peaks in well tracer 1 at 144 and 198 kPa. (B) Pressure histories ID by tracers 2, 8, 14, and 20 along column b showed a drop in input pressure from 152 to 118 kPa across the well plate, followed by sequential reflected pressures of strength 122 kPa. (C) Pressure histories ID by tracers 1 and 24 showed input pressure drop from 150 kPa in first well to 105 kPa in the 24th well ID by tracer 24.**

3.2 Experimental Results of Pressure Loading on Cells from Shock Tube and Blast Experiments

The shock tube used in our experiments generated a blast wave with a significantly longer impulse than that from the small-scale explosives. Figure 8 shows a typical pressure trace from a shock tube (pressure trace measured in air) and explosive (pressure trace measured in water) with the same peak pressure taken from this set of experiments. The duration of the pressure pulse from the explosive was 0.1 ms, whereas the duration from the shock tube was 6 ms. Table 1 displays average peak pressure and impulse data for the shock tube and explosive blast experiments. The peak pressures were not statistically different, but the impulses were over an order of magnitude larger for the shock tube blasts compared to the explosive blasts.
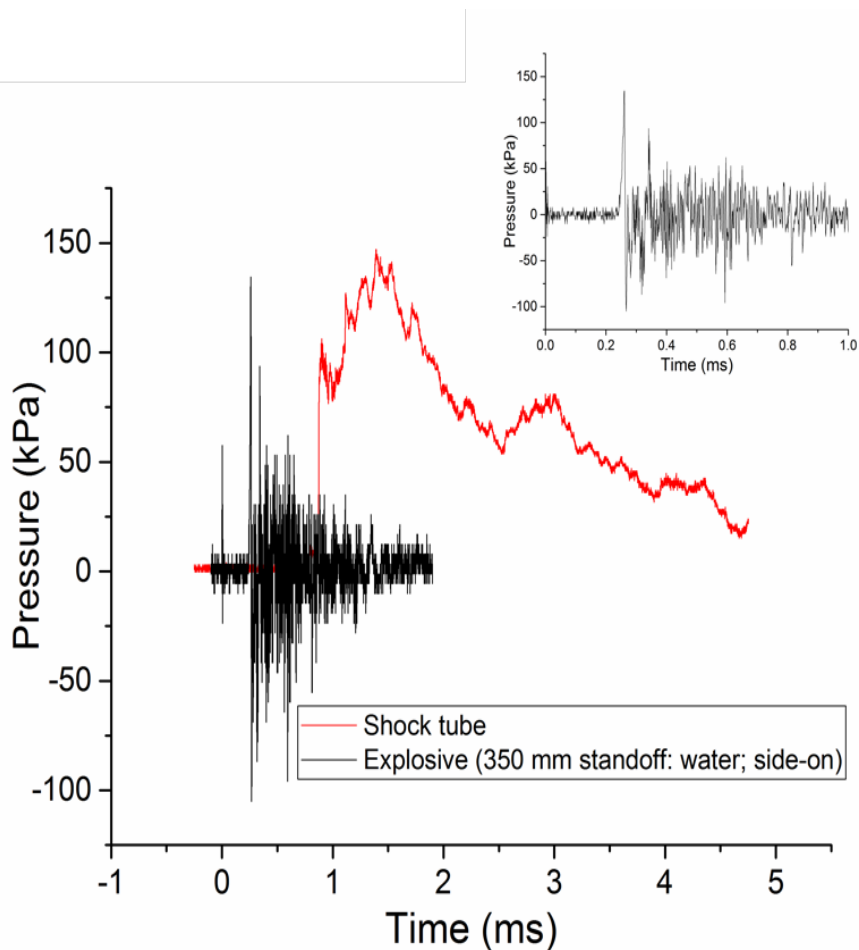
Fig. 8   Representative pressure traces for air-driven shock tube and open-air explosive in water (350-mm standoff; side on pressure). Inset is open-air explosive in water (350-mm standoff; side on pressure).

Table 1   Peak pressure and impulse averages of shock tube and explosive blast experiments

Blast source	Peak Pressure (kPa)	Impulse (kPa·ms)
Shock tube	152.1 ± 11.4	351.3 ± 46.7
Explosive[a]	125.5 ± 24.5	24.8 ± 5.4

[a] 350-mm standoff distance

One of the potential mechanisms of injury examined and observed in our in vitro model development was membrane permeability changes. Increased membrane permeability can lead to cytosketal damage due to disruption of ion homeostasis and osmotic swelling.[29,30] Figure 9 shows results from a membrane permeability assay using calcein, a 660-Da membrane impermeable dye commonly used to assess mechanoporation. The single explosive blast was found to significantly increase membrane permeability compared to the sham. The repeated explosive blast shots did not yield an uptake of calcein that was significantly different from the single explosive blast or sham conditions. The differences between the single and repeated explosive blast, however, were not significantly different. For the shock tube, both the single and the triple shots showed increased membrane permeability compared to the sham. In most cases, the sham from the shock tube and open air explosive experiments was significantly different, although every attempt was made to minimize differences (identical handling procedures, fluorescent dyes, imaging conditions). This may be due to slight variations in the cells and instrument sensitivity since the experiments were done on different days. To account for these differences, single and triple shot data were normalized to its respective sham and displayed in Table 2. A significant difference was observed between both the single and triple blasts from the shock tube and the open air explosives. The membrane permeability was 2 to 3 times higher for the cells exposed to wave fronts generated by shock tube than those subjected to open-air explosives. While membrane permeability change was not necessarily indicative of damage, an increased number of openings in the membrane could lead to intracellular ionic imbalance and the resulting damage pathways mentioned previously. It is likely that longer-term studies would see a greater effect of the membrane compromise derived either from the shock tube or explosive blast exposure, as many of the damage pathways progress slowly and may not be observed in a 24-h time frame.
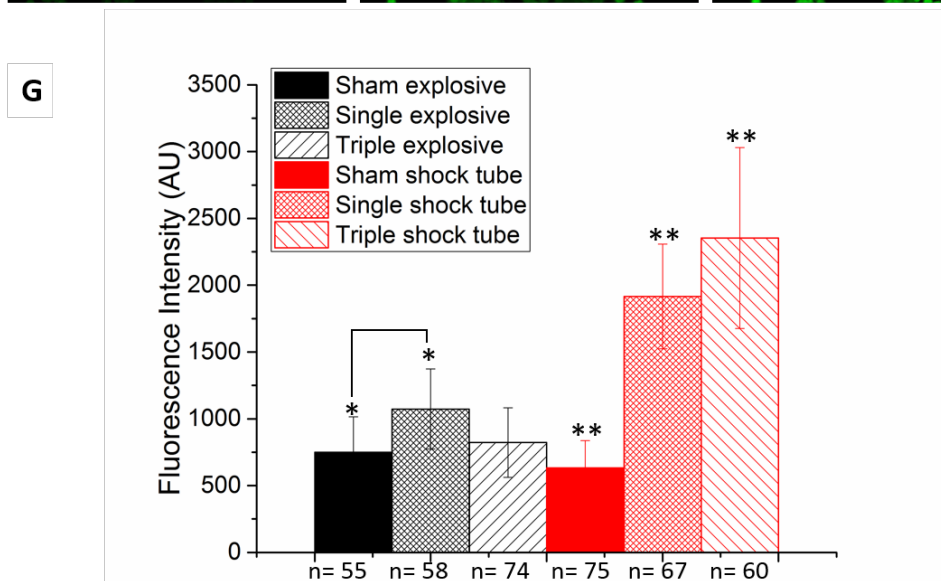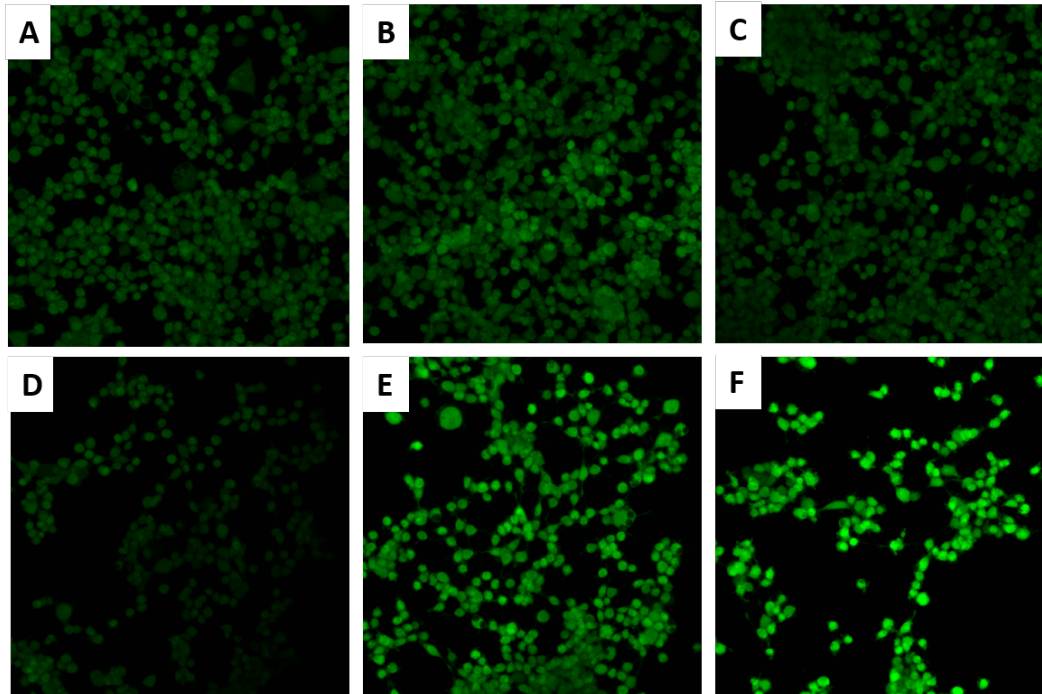
Fig. 9   Membrane permeability changes as a function of calcein dye uptake of NG108-15 cells 24 h after exposure to blast (~140 kPa). Confocal laser-scanning images of cells exposed to blast: (A) explosive sham, (B) single explosive blast, (C) triple explosive blast, (D) shock tube sham, (E) single shock tube, (F) triple shock tube, and (G) fluorescence intensity quantification. Image sizes are 640 × 640 μm. *p < 0.05 significantly different, **p < 0.05 significantly different.

Table 2   Normalized cellular assay data

Sample	Membrane permeability		Intracellular calcium		Intracellular sodium		Oxidative stress	
	n	Normalized[a]	*n*	Normalized[a]	*n*	Normalized[a]	*n*	Normalized[a]
Explosive (sham)	55	1.00	105	1.00	53	1.00	49	1.00
Explosive (s)	58	1.43 ± 0.4[b]	80	1.35 ± 0.6	53	1.27 ± 0.5[b]	74	1.97 ± 1.1[b]
Explosive (t)	74	1.09 ± 0.3[c]	95	1.23 ± 0.83[c]	55	1.47 ± 0.6[c]	79	2.94 ± 1.9[c]
Shock tube (sham)	75	1.00	63	1.00	26	1.00	68	1.00
Shock tube (s)	58	3.02 ± 0.6	71	1.58 ± 0.7	41	1.52 ± 0.4	90	2.73 ± 1.5
Shock tube (t)	74	3.72 ± 1.1	47	2.59 ± 0.8	61	1.76 ± 0.5	80	3.98 ± 1.9

[a] Normalized to sham; (s) = single blast, (t) = triple blast.
[b] Significantly different from shock tube single blast (p< 0.05).
[c] Significantly different from shock tube triple blast (p< 0.05).

To investigate the effect of the blast waves on intracellular ionic concentrations, intracellular calcium and sodium ions were probed using Fluo-4 and CoroNa Green indicators, respectively. Figure 10 displays the results from the intracellular calcium assay. The single and triple shots from the explosive blast led to significantly higher intracellular calcium compared to the sham cells, but there was no significant difference between the single and triple shots. It was anticipated that repeated explosive blast would mean more release of calcium ions. Ravin et al. found that calcium ion release has been closely linked to shear stress.[31] Cells exposed to pressures as high as ca. 1380 kPa that did not experience shear forces did not release significant amounts of calcium ions. The authors concluded that the main mechanism of damage is likely due to shear and not the compression and tension forces from the shock wave alone. In our previous work, we noticed similar results likely due to minimal shear observed in our open-air explosive blast model, in which monolayers of cells were well adhered to the bottom of the well plate. Some uptake of calcium ions from the extracellular medium due to membrane poration was expected. Since there was no significant difference in membrane perforations between single and repeated blast, the extracellular calcium ion uptake was not significant between the 2 conditions. NG108-15 cells were a fusion of neuroblastoma and glioblastoma, which make the culture more robust than a monoculture of neurons due to their neuroprotective functions. Hence, 3 blasts of ca. 140 kPa may not be above the threshold for significant calcium ion release for this cell line. Arun et al. found that this cell line was less susceptible to damage from shock tube blast waves compared to a purely neuronal cell line.[10]
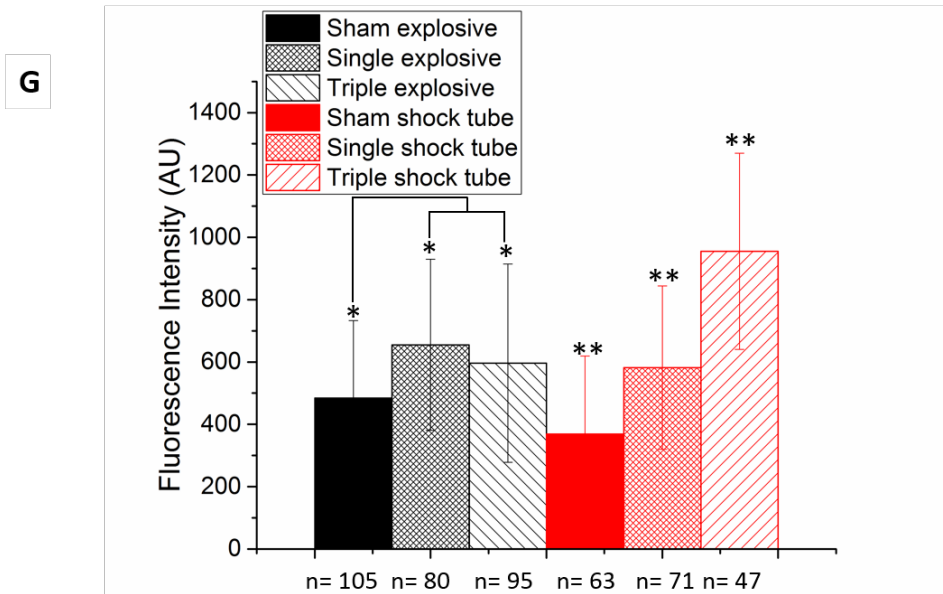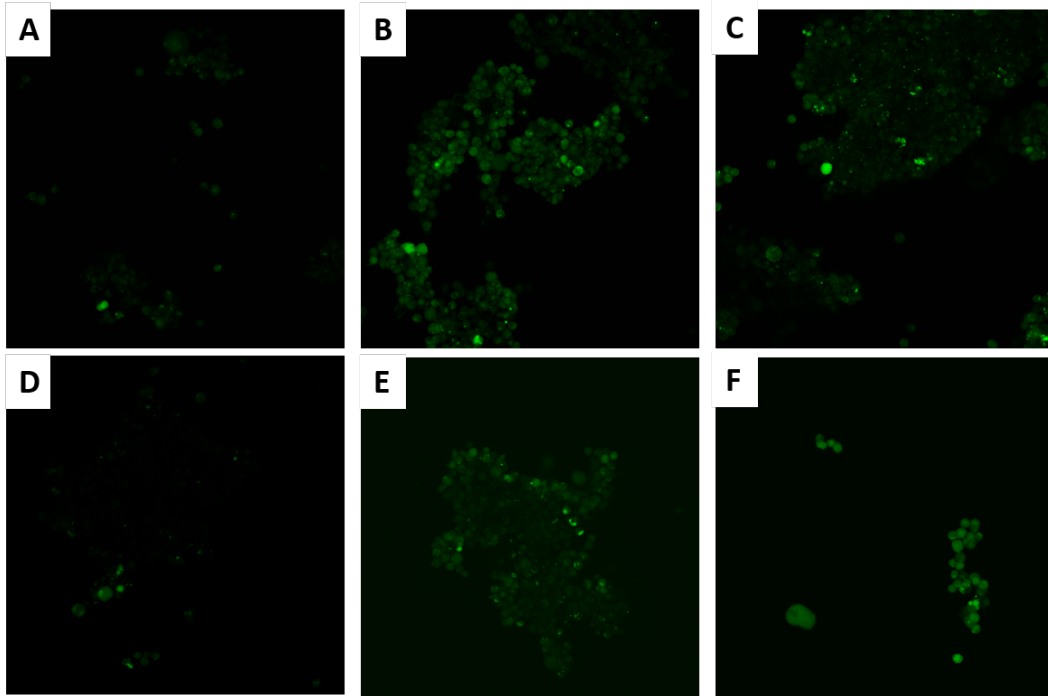
Fig. 10 Intracellular calcium measured by Fluo-4 indicator of NG108-15 cells exposed to explosive blast (~140 kPa). Confocal laser scanning images of cells exposed to blast: (A) explosive sham, (B) single explosive blast, (C) triple explosive blast, (D) shock tube sham, (E) single shock tube, (F) triple shock tube, and (G) fluorescence intensity quantification. Image sizes are 640 × 640 μm. *p < 0.05 significantly different, **p < 0.05 significantly different.

For the shock tube, single and triple shots were significantly different from the sham and each other. The triple shock tube blast was also found to be significantly higher than the triple (and single) explosive blast (Table 2). This was expected since the blast shock tube impulse (overpressure vs. positive phase time) was significantly greater than the total impulse sustained by the cells in the water tank exposed to explosive blast, and although not evaluated here, shear was anticipated to be higher in the shock tube model based on the observance of movement of the sample in the shock tube during the blast. This was not observed for the samples exposed to open air explosives using the identical sample holder. The movement of the pressurized air in the shock tube seemed to combine blast with acceleration as probable injury mechanisms, while the explosive blast experiment appeared to have minimal or no movement, with primary blast being the probable source of injury mechanisms. Acceleration/movement was only inferred from recorded videos observed during the experiment and not quantified. It is speculated that the samples in the shock tube were subjected to higher shear stress, and this in part also explained the increased membrane damage observed from the calcein assay. Rapid stretching and contraction of the membrane, a viscoelastic material, can lead to deformation of the membrane including formation of holes/pores and rupture.[32]

Figure 11 displays the results from the intracellular sodium assay. The single and triple shots for both explosive and shock tube were significantly different from each other, respectively, and from their respective shams. Intracellular sodium ion influx was also increased for both the single and triple shock tube blast compared to single and triple explosive blasts, respectively (Table 2). Sodium ion uptake depends more on membrane permeability than mechanical shear, although as discussed previously, they can be coupled. In the case of cells exposed to explosive blast, membrane permeability, as measured by the uptake of calcein dye, did not increase with repeated blast, but sodium ion uptake did. This is most likely explained by the different sizes of the dye molecules versus sodium ions (660 g/mol for calcein vs. 22 g/mol for sodium ions), and/or stimulation of the mechanosensitive ion channels allowing the selective passage of sodium ions.
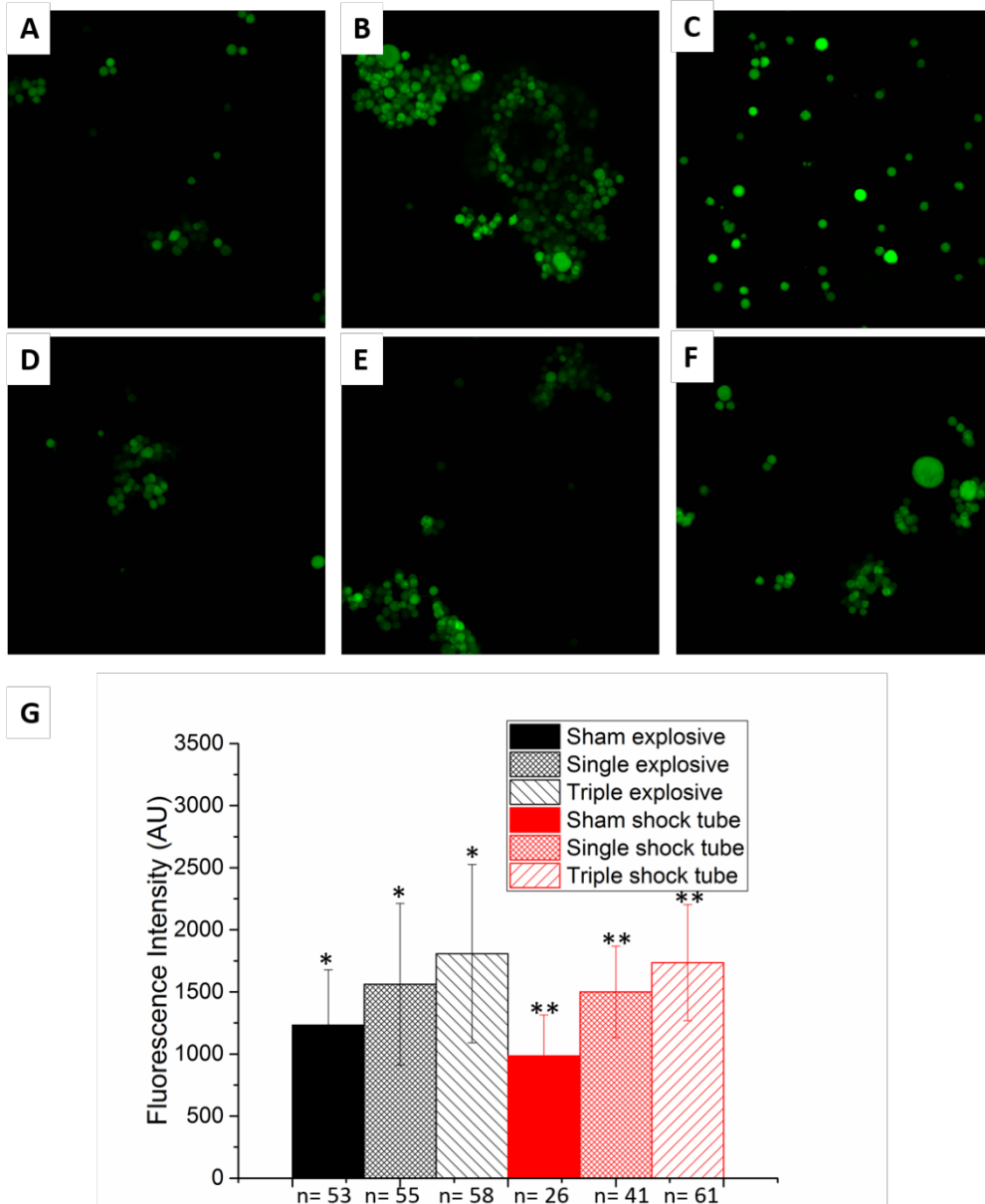
Fig. 11   Intracellular sodium measured by CoroNa Green indicator of NG108-15 cells exposed to explosive blast (~140 kPa). Confocal laser scanning images of cells exposed to blast: (A) explosive sham, (B) single explosive blast, (C) triple explosive blast, (D) shock tube sham, (E) single shock tube, (F) triple shock tube, and (G) fluorescence intensity quantification. Image sizes are 640×640 μm. *p < 0.05 significantly different.

The formation of reactive oxygen species or an increase in oxidative stress was probed using a nonfluorescent acetylated form of fluorescein. The dye is converted to a green-fluorescent form when the acetate groups are cleaved by intracellular esterases and oxidation. The single and triple shots for both explosive and shock tubes were significantly different from each other, respectively, and from their

respective shams (Fig. 12). Oxidative stress was also increased for both the single and triple shock tube blast compared to single and triple explosive blasts, respectively (Table 2).
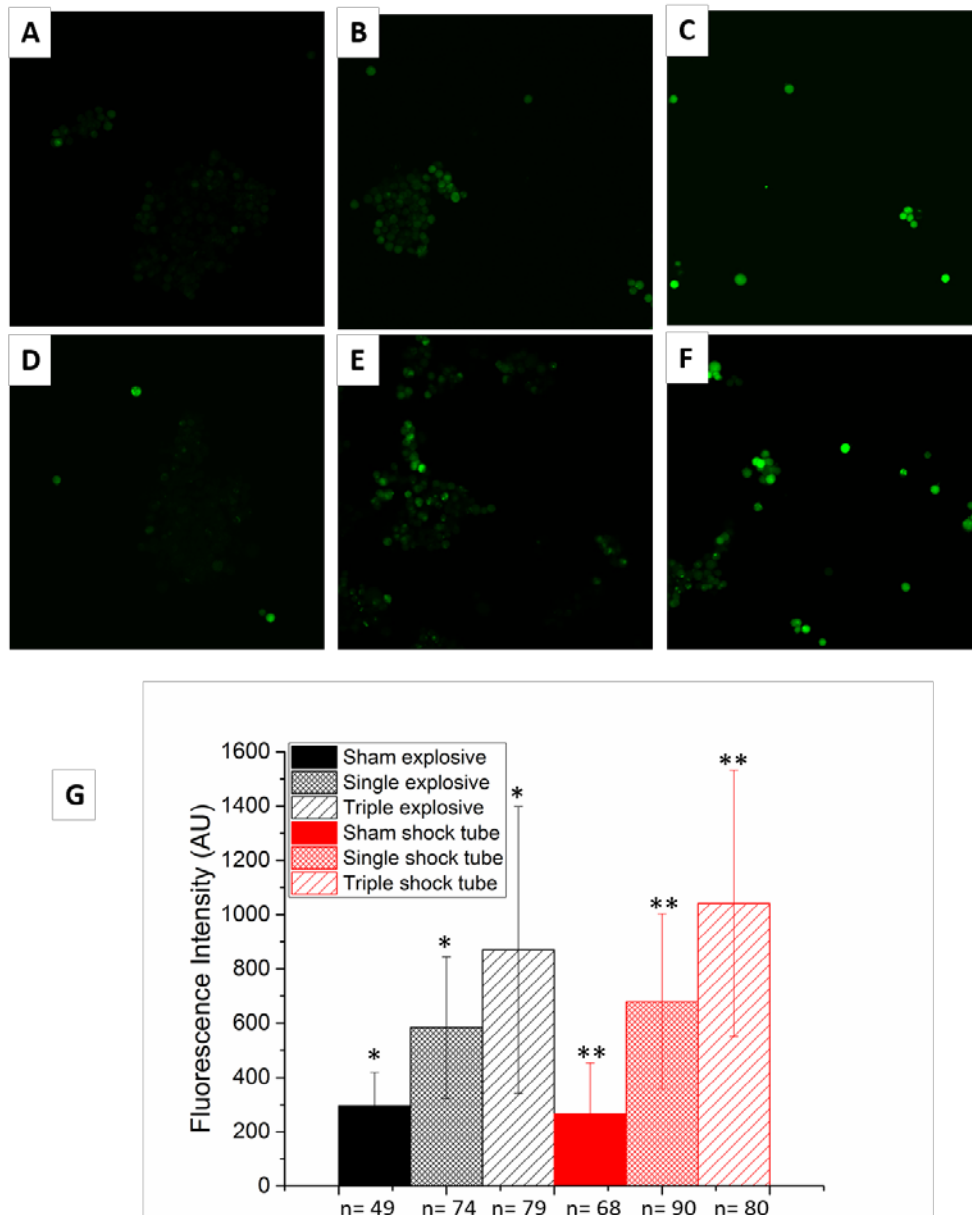
Fig. 12   Reactive oxygen species changes as a function of ROS indicator uptake of NG108-15 cells exposed to explosive blast (~140 kPa). Confocal laser scanning images of cells exposed to blast: (A) explosive sham, (B) single explosive blast, (C) triple explosive blast, (D) shock tube sham, (E) single shock tube, (F) triple shock tube, and (G) fluorescence intensity quantification. Images sizes are 640 × 640 μm. *p < 0.05 significantly different, **p < 0.05 significantly different.

4.   Conclusions

In this work, NG108-15 cells were subjected to blast generated by a shock tube and from open-air explosives at the same peak pressure. Every effort was made to keep the conditions identical in terms of sample handling and holders. For the open-air blast, the cell plates were submerged in a tank of water, while the shock tube experiments were done in air. Furthermore, the open-air explosive blast had a much shorter duration than the shock tube blast because of the small size of the explosive charge. Thus, the longer duration of exposure in the shock tube experiments may lead to more indicators of damage such as those we observed in our experiments.

Although we observed that shock tube blasts led to increased indicators for damage such as membrane perforation, disruption of ionic homeostasis, and increased oxidative stress, more research is warranted. Performing the explosive experiments in air would be a suitable means for direct comparison to those in the shock tube, as well as to the bioeffects we observed in the water tank model. In addition, using an explosive with a blast wave duration more closely matched to that of the shock tube would further aid in the deconvolution of the effects of duration, negative pressure, and reflected shock waves. Later data collection time points would also aid in understanding the impact of the damage mechanism precursors observed and enable further knowledge of whether they lead to decreased cellular function or death. In addition, although reflections of the blast wave occur within the head when impacted, they are likely not the same as those predicted to occur in the well plate. A more accurate in vitro model that better resembles the skull and skin would be advantageous. Validation with animal studies is critical to link plausible cell damage mechanisms to injury. This knowledge of loading conditions and injury pathways will greatly aid in better designed experiments that more closely mimic the blast conditions to which Soldiers and civilians are exposed. This is also critical for proper designing and testing of protective equipment, diagnosis, and treatment of traumatic brain injuries.

5. References

1. Williamson V, Mulhall E. Invisible wounds: psychological and neurological injuries confront a new generation of veterans. Iraq and Afghanistan Veterans of America. 2009 Jan [accessed 2016 Oct 19]. http://issuu.com/iava/docs/invisible_wounds_2009.

2. Brethauer SA, Chao A, Chambers LW, Green DJ, Brown C, Rhee P, Bohman HR. Invasion vs insurgency: US Navy/Marine Corps forward surgical care during Operation Iraqi Freedom. Arch Surg. 2008;143:564–569.

3. Wade AL, Dye JL, Mohrle CR, Galarneau MR. Head, face, and neck injuries during Operation Brain Injuries from Blast 201 Iraqi Freedom II: results from the US Navy-Marine Corps Combat Trauma Registry. J Trauma. 2007;63:836–840.

4. Zouris JM, Walker GJ, Dye J, Galarneau M. Wounding patterns for US Marines and sailors during Operation Iraqi Freedom, major combat phase. Mil Med. 2006;171:246–252.

5. Ning Y; Zhou Y. Shock tubes and injury modeling. Chin J Traumatol. 2015;18:187–193.

6. Bass CR, Panzer MB, Rafaels KA, Wood G, Shridharani J, Capehart B. Brain injuries from blast. Ann Biomed Eng. 2011;40:185–202.

7. Needham, CE, Ritzel D, Rule GT, Wiri S, Young L. Blast testing issues and TBI: experimental models that lead to wrong conclusions. Front Neurol. 2015;6:72.

8. Chen Y, Constantini S. Caveats for using shock tube in blast-induced traumatic brain injury research. Front Neurol. 2013;4:117.

9. Sawyer TW, Wang Y, Ritzel DV, Josey T, Villanueva M, Shei Y, Nelson P, Hennes G, Weiss T, Vair C, et al. High-fidelity simulation of primary blast: direct effects on the head. J Neurotrauma. 2016;22:1181–1193.

10. Arun P, Spadaro J, John J, Gharavi RB, Bentley TB, Nambiar MP. Studies on blast traumatic brain injury using in vitro model with shock tube. Neuroreport. 2011;22:379–384.

11. Reneer DV, Hisel RD, Hoffman JM, Kryscio RJ, Lusk BT, Geddes JW. A Multi-mode shock tube for investigation of blast-induced traumatic brain injury. J Neurotrauma. 2011;28:95–104.

12. Hue CD, Cho FS, Cao S, Nicholls RE, Vogel EW, Sibindi C, Arancio O, Bass CR, Meaney DF, Morrison B. Time course and size of blood–brain barrier opening in a mouse model of blast-induced traumatic brain injury. J Neurotrauma. 2016;33:1202–1211.

13. Effgen GB, Hue CD, Vogel E, Panzer MB, Meaney DF, Bass CR, Morrison B. A multiscale approach to blast neurotrauma modeling: part II: methodology for inducing blast injury to in vitro model. Front Neuro. 2012;3:1–10.

14. Chandra N, Ganpule S, Kleinschmit NN, Feng R, Holmberg AD, Sundaramurthy A, Selvan V, Alai A. Evolution of blast wave profiles in simulated air blasts: experiment and computational modeling. Shock Waves. 2012;22:403–415.

15. Bleakney W, Taub AH. Interaction of shock waves. Rev Mod Phys. 1949;21:584–605.

16. Sawyer TW, Wang Y, Ritzel DV, Josey T, Villanueva M, Shei Y, Nelson P, Hennes G, Weiss T, Vair C, et al. High-fidelity simulation of primary blast: direct effects on the head. J Neurotrauma. 2016;33:1181–93.

17. Patel TP, Ventre SC, Geddes-Klein D, Singh PK, Meaney DF. Single-neuron NMDA repector phenotype influences neuronal rewiring and reintegration following traumatic injury. J Neurosci. 2014;34:4200–4213.

18. Shenton ME, Hamoda HM, Schneiderman JS, Bouix S, Pasternak O, Rathi Y, M-A V, Purohit MP, Helmer K, Koerte I, et al. A review of magnetic resonance imaging and diffusion tensor imaging findings in mild traumatic brain injury. Brain Imaging Behav. 2012;6:134–192.

19. LaPlaca MC, Prado GR, Cullen D, Simon CM. Plasma membrane damage as a marker of neuronal injury. Conf Proc IEEE Eng Med Biol Soc; 2009. p. 1113–1116.

20. Geddes DM, Cargill RS, LaPlaca MC. Mechanical stretch to neurons results in a strain rate and magnitude-dependent increase in plasma membrane permeability. J Neurotrauma. 2004;20:1039–1049.

21. LaPlaca MC, Prado GR. Neural mechanobiology and neuronal vulnerability to traumatic loading. J Biomech. 2010;43:71–78.

22. Smith DH, Meaney DF. Axonal damage in traumatic brain injury. Neuroscientist. 2000;6:483–495

23. Monnerie H, Tang-Schomer MD, Iwata A, Smith DH, Kim HA, Le Roux PD. Dendritic alterations after dynamic axonal stretch injury in vitro. Exp Neurol. 2010;224:415–423.

24. Prasad KN, Bondy SC. Common biochemical defects linkage between post-traumatic stress disorders, mild traumatic brain injury (TBI) and penetrating TBI. Brain Res. 2015;1599:103–114.

25. Zander NE, Piehler T, Boggs M, Banton R, Benjamin R. In vitro studies of primary explosive blast loading on neurons. J Neurosci Res. 2015;931353–1363.

26. Zander NE, Piehler T, Banton R, Boggs M. The effect of explosive blast loading on human neuroblastoma cells. Anal Biochem. 2016;504:4–6.

27. Hertel ES, Bell RL, Elrick MG, Farnsworth AV, Kerley GI, McGlaun JM, Petney SV, Silling SA, Taylor PA, Yarrington L. CTH: a software family for multi-dimensional shock physics analysis. Proceedings of the 19th International Symposium on Shock Waves; 1993 July 26–30; Marseille, France. p. 377–382.

28. Hertel ES, Kerley GI. CTH reference manual: the equation of state package. Albuquerque (NM); Sandia National Laboratories (US); 1998. Report No.: SAND98-0947.

29. Kilinc D, Gallo G, Barbee KA. Mechanically-induced membrane poration causes axonal beading and localized cytoskeletal damage. Exp Neurol. 2008;212:422–430.

30. Monnerie H, Tang-Schomer MD, Iwata A, Smith DH, Kim HA, Le Roux PD. Dendritic alterations after dynamic axonal stretch injury in vitro. Exp Neurol. 2010;224:415–423.

31. Ravin R, Blank PS, Steinkamp A, Rappaport SM, Ravin N, Bezrukov L, Guerrero-Cazares H, Quinones-Hinojosa A, Bezrukov SM, Zimmerberg J. Shear forces during blast, not abrupt changes in pressure alone, generate calcium activity in human brain cells. PLOS One. 2012;7: e39421.

32. Arwarz G, Smits AJ. A viscoelastic model of shear-induced hemolysis in laminar flow. Biorheology. 2012;50:45–55.

List of Symbols, Abbreviations, and Acronyms

2-D	2-dimensional
ABS	Advanced Blast Simulator
AMR	adaptive mesh refinement
EOS	equation of state
mTBI	mild TBI
PBS	phosphate-buffered saline
PMMA	polymethylmethacrylate
RDX	cyclotrimethylene trinitramine
ROS	reactive oxygen species
TBI	traumatic brain injury

1 (PDF)	DEFENSE TECHNICAL INFORMATION CTR DTIC OCA
2 (PDF)	DIR ARL IMAL HRA RECORDS MGMT RDRL DCL TECH LIB
1 (PDF)	GOVT PRINTG OFC A MALHOTRA
4 (PDF)	ARL RDRL WMM G N E ZANDER R BANTON RDRL WML C T PIEHLER R BENJAMIN